Pergamon

Int. J. Heat Mass Transfer. Vol. 37, No. 15, pp. 2261–2271, 1994

0017–9310/94 $7.00 + 0.00

0017–9310(94)E0037–U

The turbulent boundary layer over single V-shaped grooves

S. C. TANTIRIGE,† A. P. IRIBARNE,‡ M. OJHA§ and O. TRASS‡¶

†Idea Research, Toronto
‡Department of Chemical Engineering and Applied Chemistry and §Institute of Biomedical Engineering, University of Toronto, Toronto, Ontario, Canada M5S 1A4

(*Received* 8 *June* 1993 *and in final form* 10 *January* 1994)

Abstract—The photochromic tracer technique was used to study the turbulent boundary layer over two transverse V-shaped grooves. The mean velocity profiles above the individual grooves were parallel to those seen in the outer regions for smooth surfaces, but displaced downwards. Also, the turbulence intensity just above the grooves was higher than the corresponding smooth surface values. These results suggest that enhancement of heat and mass transfer rates by transverse grooves is due to energetic bursts which effectively replace the liquid within the groove, with a contribution from an apparent increase in burst frequency.

INTRODUCTION

THE ENHANCEMENT of heat and mass transfer rates by surface roughness is caused by increased turbulent transport which leads to a concurrent increase in drag. In order to contribute to the optimization of heat and mass transfer processes, some aspects of the underlying momentum transfer mechanism are investigated in this study.

For turbulent flow over smooth surfaces, the heat and mass transfer rates are apparently influenced by the turbulent bursting process [1]. This phenomenon has been investigated quite actively since the major pioneering work conducted by Kline *et al.* [2]. They used the hydrogen bubble technique to show the presence of coherent structures within the viscous sublayer and the subsequent ejection of these structures into the outer region of the boundary layer. The Reynolds stresses and the turbulent energy production were shown to be strongly correlated with the periodic ejection of the low-velocity fluid from the near-wall region [3–5]. The bursting process appears to involve a long region or streak of low-speed fluid within the viscous sublayer that remains stable for some streamwise distance [6]. The streak then lifts upwards and oscillates before being ejected away from the wall in a coherent manner. Acalar and Smith [7] suggested the lift-up phase of the low speed streak leads to the formation of a hairpin vortex and the ejection phase, and eventually to the re-development of another low-speed streak. The complete process is referred to as a burst, and results in the inrush of high-velocity fluid into the wall region [8].

The phrase "turbulent bursting" was coined by Kim *et al.* [4], and it is widely believed that the periodic bursting process is the predominant mode of turbulence production. The discovery of these coherent structures within the turbulent boundary layer led to the idea of drag reduction using surfaces with longitudinal grooves or riblets [9]. It was observed that the size of the grooves should be comparable to that of the viscous sublayer. Extensive research has been carried out in this area of turbulence manipulation as reported by Choi [10]. In addition, Choi has postulated that the restriction of the spanwise movement of the legs of the hairpin vortices (associated with turbulent bursting) results in premature bursts and leads to a reduction in the turbulent skin friction. This condition is also achieved with drag reducing polymers which cause a substantial reduction in convective heat transfer [11].

There are situations where enhancement of heat transfer is required such as in turbine cooling channels and heat exchangers [12,13], or of mass transfer as in electrodialysis and artificial kidney systems [14]. This is normally achieved through the use of rib turbulators or baffles positioned in the spanwise direction to increase the transfer surface area and to promote turbulence. Some of the factors that affect the transfer coefficients and the friction factor are orientation, height and spacing of the protrusion, aspect ratio of the channel, and Reynolds number. In general, it was found that, for constant pumping power, specific configurations of the geometric factors could lead to more efficient transfer.

The main reason for investigating V-shaped grooves in this study was to extend the work of Dawson and Trass [15] who found that, at high Schmidt numbers and with multiple V-shaped grooves, the mass transfer rates could be increased by a factor of 3–4 for the dimensionless roughness height e^+ of 10 or greater. Frictional resistance increased much less, typically 20–50% in the region of the maximum mass transfer rate enhancement. The objective of the present study is to

¶ Author to whom correspondence should be addressed.

NOMENCLATURE

D_e	equivalent diameter: 4 × cross-sectional area/perimeter = 25 mm	w	groove width
e	roughness height	X	distance from the upstream edge of the groove, normalized with respect to groove width
e^+	roughness Reynolds number, eu^*/v	y	normal distance
Re	Reynolds number, $D_e u/v$	y^+	dimensionless distance, yu^*/v.
T_b	burst period, mean time interval between successive bursts	Greek symbols	
u	axial velocity	μ	viscosity
u^+	dimensionless velocity, u/u^*	ν	kinematic viscosity, μ/ρ
u^*	friction velocity, $(\tau_w/\rho)^{1/2}$	ρ	density
u'	turbulence intensity = $\sqrt{(u-\bar{u})^2}/u^*$	τ_w	wall shear stress.
$\bar{u}$	mean axial velocity		

better understand the underlying physical processes responsible for the enhanced transfer rates. Because of limitations with the measurement technique as employed in this study, the groove sizes were larger than those used by Dawson and Trass [15], and the Reynolds numbers corresponded roughly to the lower end of the range used in the previous study.

The photochromic tracer technique was used to provide detailed flow visualization of the turbulent boundary layers. Flow over a smooth surface was first investigated in order to evaluate the accuracy of the non-disturbing photochromic tracer technique in determining the velocity profiles within the turbulent boundary layer, and also to aid in the interpretation of the rough surface results. The visualization method was developed at the University of Toronto by Popovich and Hummel [16] who provided convincing evidence on the dynamic behavior of the viscous sublayer. They found that the thickness of the sublayer fluctuated quite intensely, achieving a minimum value of $y^+ = 1.6$ and an average thickness similar to the widely accepted value of 5.0. The method has since been applied quite successfully in other studies using steady [17–19] and unsteady [20, 21] flow conditions.

METHODS

The photochromic tracer technique as used in this study has been described in detail elsewhere [16–18]. In essence, it involved the use of a photochromic dye, 1′3′3′-trimethylindoline-6-nitrobezospiropyran dissolved in deodorized kerosene at a concentration of 0.01% by weight. Upon irradiation with a focused beam of uv light from an Argon laser, a dark blue trace was produced in the colorless solution in less than one microsecond. Thus, under the flow conditions used in the present study, the initial shape of the trace was a straight line. Its displacement profile was then photographed with a 16 mm Hycam (up to 5000 frames s^{-1}) or Locam (up to 500 frames s^{-1}) movie camera, depending on the local velocities within the test region. In each experiment, spot-marks were placed on the film at a rate of 100 Hz in order to calculate the actual framing rate. Maximum film contrast was achieved with the use of Kodak Technical Pan film together with yellow background illumination from a high-pressure sodium lamp.

The flow loop and the test section are sketched in Fig. 1a and b. The single V-shaped grooves were carefully machined on special quartz sheets (test surfaces) for high transmittance of the uv light, and the sides of the grooves were polished to reduce optical distortion and surface roughness. A 25 mm square channel made from transparent Lucite served as the test section such that the test side (surface) could be replaced. In order to achieve high Reynolds numbers,

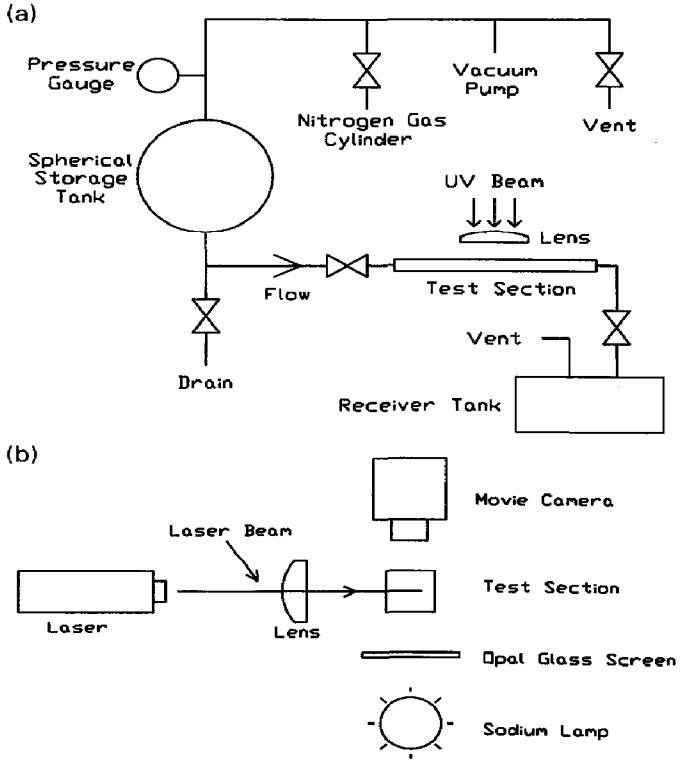

FIG. 1. Schematic diagram of (a) the flow loop and (b) the test-section.

the head tank was pressurized with nitrogen gas. An entrance length of 120 channel heights was used to ensure fully developed flow at the test section.

Axial velocities were determined from the displacement of the trace over the time interval of successive photographic frames. The dye trace in each frame was digitized using a Tektronix 4956 digitizing tablet interfaced to a Tektronix 4051 computer. The photographic film was first projected onto the digitizing tablet and the x, y-coordinates of the trace were obtained with the use of a magnetic cursor. In calculating the velocities, it was assumed that the displacement due to the velocity component normal to the surface of the channel was insignificant. For flow within the viscous sublayer, this assumption is quite valid since the flow is essentially unidirectional. Outside the viscous sublayer, the error introduced by the non-axial motions was minimized by using very small intervals between consecutive photographic frames. In calculating the mean axial velocities, this error was further minimized due to the averaging of the effects from the positive and negative values of the non-axial velocities. However, in determining the turbulence intensity, the error can be significant outside the viscous sublayer. As mentioned earlier, the smooth surface results will be used to further assess the overall accuracy of these velocity measurements.

A total of about 30 traces was recorded for each set of test conditions. Each trace remained visible on four consecutive photographic frames and these were digitized in order to obtain the axial velocities. Figure 2 shows the shape and dimensions of the two grooves, the initial position of the dye traces and the Reynolds numbers. The traces were positioned at the three locations in order to examine the effects on the velocity field around the groove. Since the trace was displaced over a finite distance during the data acquisition interval, the velocity data will correspond to a location at some intermediate position between the initial and final positions of the dye trace. That is, the data would represent the average Lagrangian values over the distance traveled by the trace. It should be noted that the friction velocity for both the smooth surface and the surfaces with the single V-shaped grooves were calculated from the Blasius resistance formula for turbulent flow through smooth pipes [22]. Further experimental and analytical details are reported by Tantirige [23].

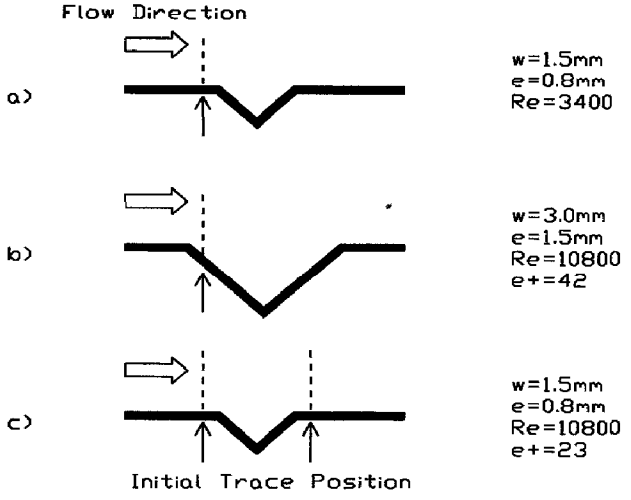

FIG. 2. Groove shapes and initial dye trace positions, with the Reynolds numbers reported.

RESULTS

Smooth surface

The Reynolds number used with the smooth surface was 39 500 and a sequence of the trace displacement profiles (time lines) at 0.3 ms intervals is shown in Fig. 3. The high shearing of the trace within the viscous sublayer and its deformation within the buffer zone

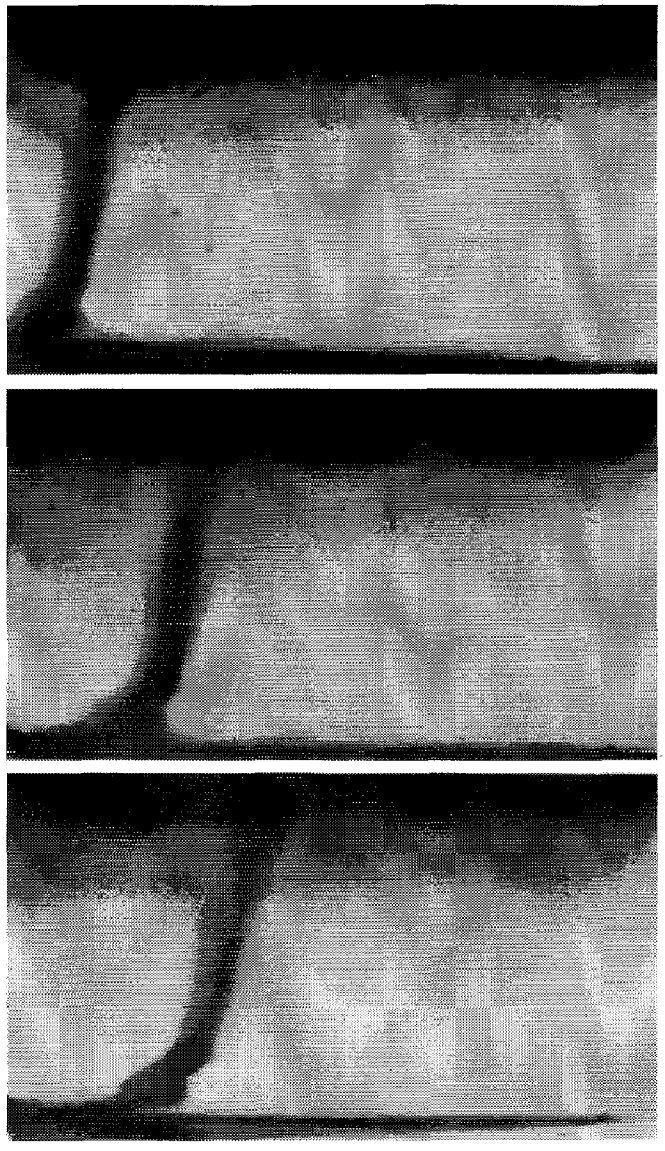

FIG. 3. Smooth surface: displacement of the dye trace for $Re = 39\,500$. Interval between consecutive frames is 0.3 ms.

are quite obvious. Figure 4a shows a comparison of the mean velocity data obtained under these conditions and those predicted from the von Karman "universal velocity distribution law" [24]:

$$u^+ = y^+, \qquad y^+ \leqslant 5 \tag{1a}$$

$$u^+ = 5.0 \ln y^+ - 3.05, \quad 5 < y^+ \leqslant 30 \tag{1b}$$

$$u^+ = 2.5 \ln y^+ + 5.5, \quad y^+ > 30 \tag{1c}$$

where u^+ is the dimensionless velocity and y^+ the dimensionless distance. Overall, good agreement was observed with the von Karman equations, particularly within the transition region ($5 < y^+ \leqslant 30$), thereby confirming the reliability of the technique for the measurement of average velocity profiles.

The turbulence intensity of the axial flow is plotted against y^+ in Fig. 4b together with the results reported by Morrison and Kronauer [25] for air flow in a circular pipe and by Ueda and Hinze [26] for a low-turbulence wind tunnel. The data lie in the same range except that, in the present study, the peak value was slightly higher and closer to the wall. This deviation can be due to the square shape of the test section leading to some secondary effects, and to errors arising from the inability to accurately measure the instantaneous axial velocity in the presence of significant non-axial motion.

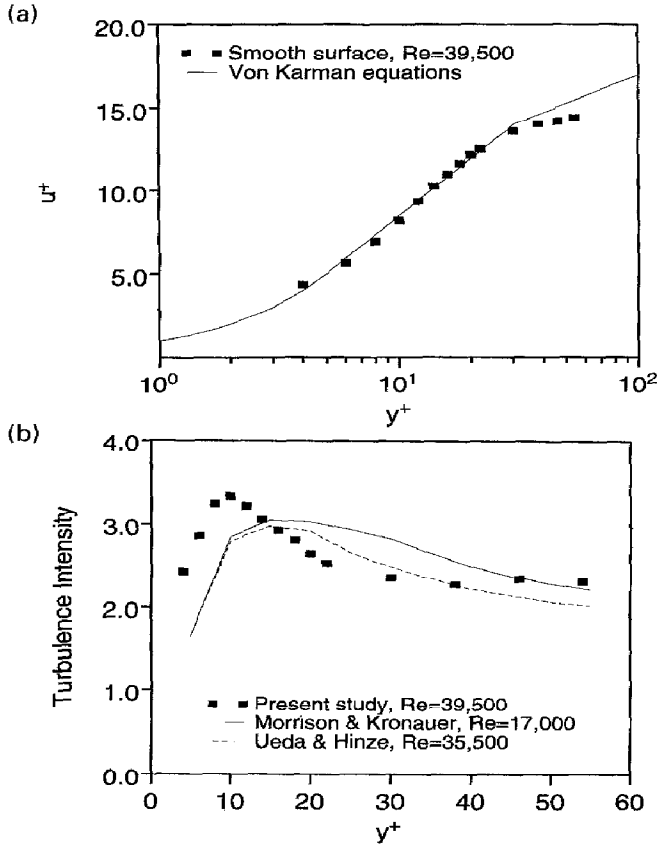

FIG. 4. Smooth surface results on: (a) the mean velocity data; and (b) the turbulence intensity profiles compared with published correlations.

Figure 5 provides further details on the axial velocity distribution at various y^+ positions across the boundary layer, again for $Re = 39\,500$. Characteristic features of the turbulent boundary layer included a skewed distribution towards the lower velocities at $y^+ = 4$ and 6, which is indicative of the highly active nature of the flow field at the edge of the viscous sublayer. In fact, this pattern is somewhat consistent with the results of Popovich and Hummel [16] who found the thickness of the viscous sublayer to strongly oscillate around an average value of $y^+ = 6.2$ with the most probable value being $y^+ = 4.3$. This would explain the slightly more bimodal distribution at $y^+ = 6.0$ compared to that at $y^+ = 4.0$. With increasing distance from the wall, the velocity distributions became more symmetric.

V-shaped grooves

Detailed information on the effects of the grooves was obtained by positioning the dye traces within, upstream and downstream of the two grooves. The initial positions of the dye traces and the flow conditions are shown in Fig. 2.

Velocity measurements. For $Re = 3400$ and with the trace position upstream of the smaller groove, the mean axial velocity data are compared with the von Karman profile in Fig. 6. Since the trace (tagged fluid) has traveled and resided mostly over the groove during the sampling time, roughly 25% of the groove width, an increase in velocity of the lower part of the trace would be expected because of the absence of the wall. However, as shown in Fig. 6a, the velocities were lower than those seen with the smooth surface. This was due to the flow field being not fully turbulent but in a transitional state as indicated by the portion of the dye trace that was further away from the wall. As expected, the turbulence intensity level in this less than fully developed flow field was significantly lower than that seen with fully developed flow over the smooth surface (Fig. 6b).

Data for the larger groove are also shown in Fig. 6. The trace was positioned within the groove and the Reynolds number was 10 800. (The trace was also positioned upstream of the groove, but the films were not satisfactory for quantitative analysis.) The upstream flow was fully turbulent and this was quite evident from the complex flow pattern seen from the photochromic dye traces. It should be noted that the point $y^+ = 0$ was considered to be at the intersection of the trace and the line joining the two corners of the groove, i.e. it was taken to be at the same height as the smooth surface. The decision to use the free surface instead of the wall of the groove was made for two reasons. First, it was based on the observation (to be discussed in detail later) that the flow within the groove was quite different from that of the mainstream flow. Second, it was done in order to assess the trend in the velocity distributions when compared with the smooth surface results at equivalent distances from the wall.

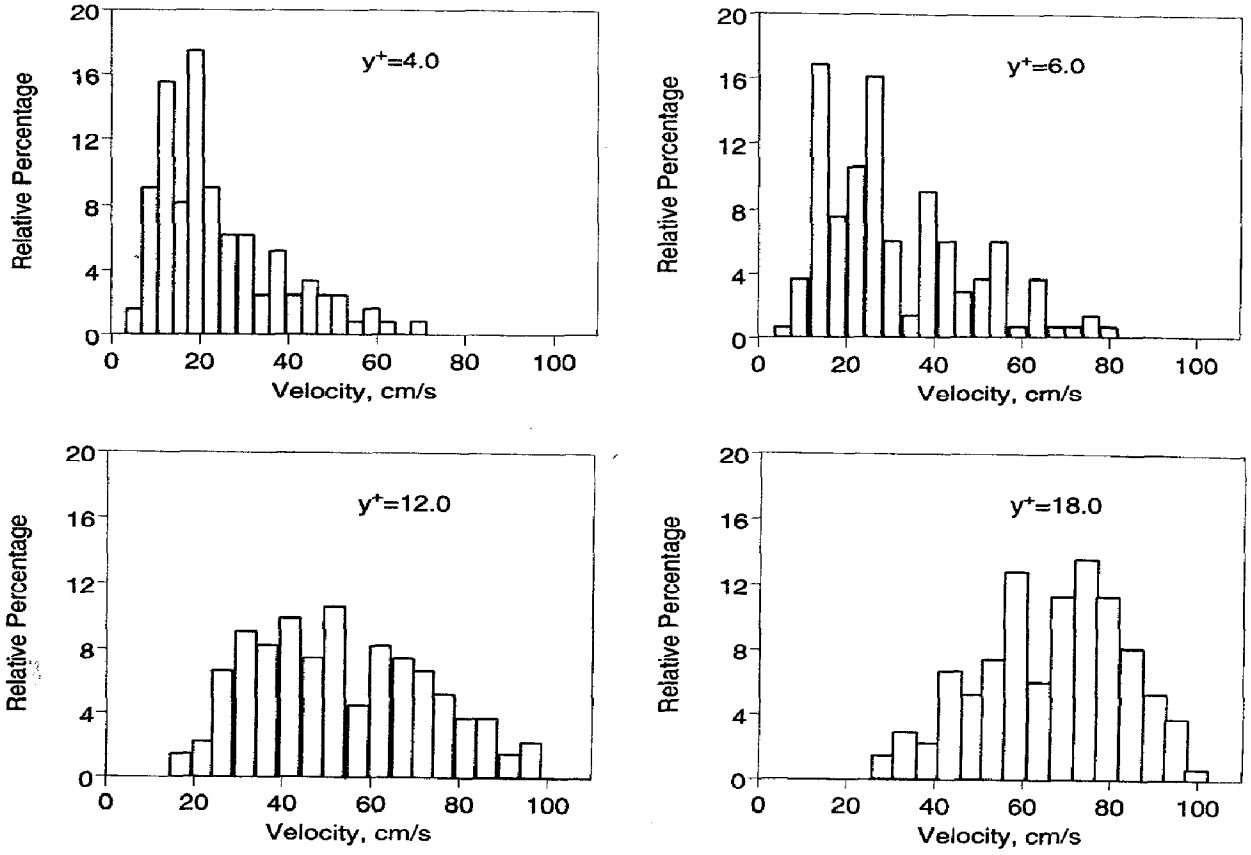

FIG. 5. Distribution of the instantaneous velocities across the wall region: smooth surface, $Re = 39\,500$.

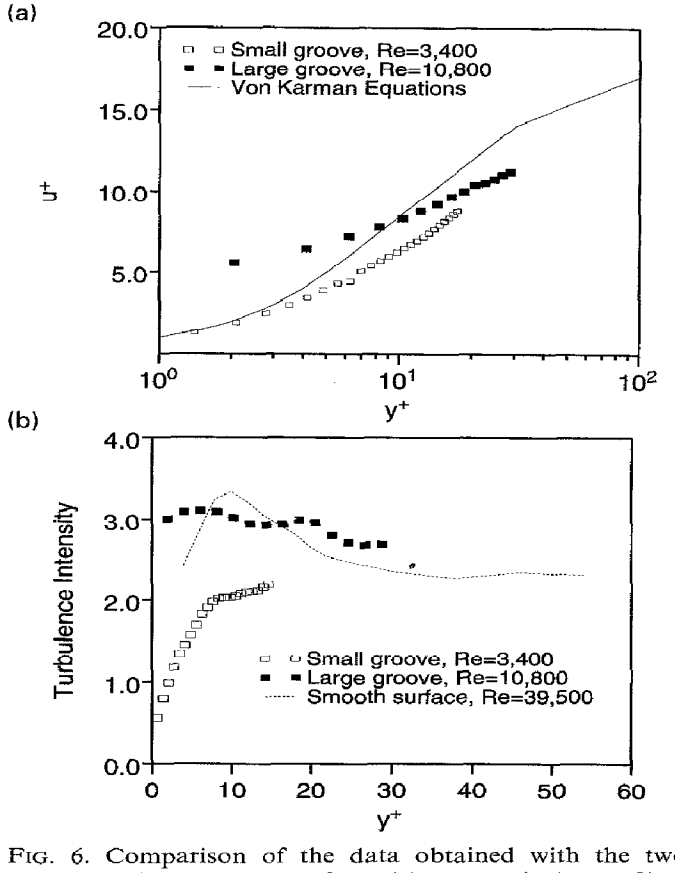

FIG. 6. Comparison of the data obtained with the two grooves and the smooth surface: (a) mean velocity profiles; and (b) turbulence intensity profiles.

The relatively uniform distribution of the turbulence intensity over the large groove for $Re = 10\,800$ (Fig. 6b) suggests that viscous effects were negligible in this region. This can explain the difference between the mean velocity distributions over the groove and for smooth surfaces as seen in Fig. 6a. The profile over the groove for $y^+ < 30$ was almost parallel to that seen with the von Karman equation in the outer region. Obviously, the higher velocities observed just above the mouth of the cavity were due to the absence of the wall.

At the same Reynolds number of 10 800, the laser beam was split such that two traces were produced with one positioned upstream and the other downstream of the smaller groove as shown earlier in Fig. 2. (Again, the quality of the films obtained with multiple traces for the larger groove was not satisfactory for quantitative analysis.) The mean velocities are compared in Fig. 7a with the von Karman universal velocity distribution. The mean velocities were higher at the upstream location in comparison to the downstream values, particularly in the region of $y^+ < 10$. This is expected since the trace introduced at the upstream location resided mostly over the groove and was not subjected to the damping effect of the wall. The trend in the results is similar to that described earlier for the larger groove, which is also shown in Fig. 7a for comparison. However, with the larger groove, the trace started from a position inside the groove and thus the velocities were higher since the

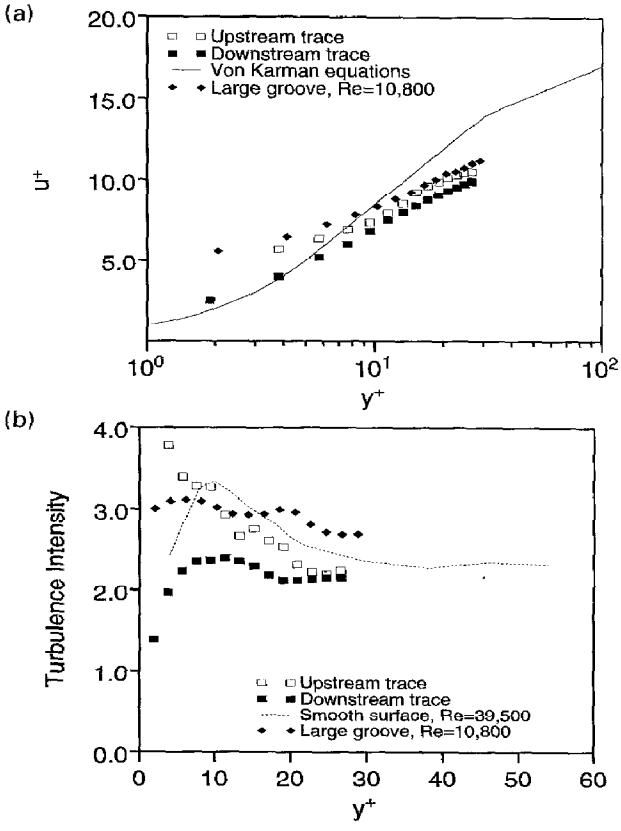

FIG. 7. (a) Mean velocity; and (b) turbulence intensity data at $Re = 10\,800$: upstream and downstream traces for the smaller groove. The results with the trace in the larger groove are also shown.

tagged fluid was less constrained compared to the upstream trace with the smaller groove.

The turbulence intensities are presented in Fig. 7b along with the data from the larger groove. The two profiles for the smaller groove appear to merge at $y^+ > 20$, which is an indication that the influence of the groove did not extend beyond this point. Closer to the wall, the turbulence intensities were larger for the upstream location which is consistent with the mean velocity data. Further, since the trace introduced at the upstream location will initially be influenced by the upstream smooth surface and then by the groove, it is possible that this combined effect can lead to larger unsteady components in the velocity and may explain the high values seen for $y^+ < 10$, compared to those with the trace positioned within the larger groove. Beyond $y^+ > 10$, the turbulence intensities were much lower than those seen with the larger groove; this may be due primarily to the difference in groove size.

Dynamics of the fluid renewal process. With laminar upstream flow at $Re = 2000$, a simple flow pattern was seen in the larger groove. It consisted of a stable vortex with relatively little fluid exchange involving fluid entrainment on the downstream end and removal in the upstream region. A complete rotation of the vortex occurred in approximately 3 s. For $Re = 3400$ and with the smaller groove, there was increased exchange of fluid between the groove and the outer region of the flow. The exchange process occurred exclusively at the downstream end of the groove, and, for the given plane of view, an inrush of fluid was seen to be followed by an ejection. The interval between successive "bursts" was quite long compared to the duration of an individual burst, and the vortex within the groove experienced several rotations before ejection occurred.

At a higher Reynolds number of 10 800 and with the larger groove, the liquid exchange occurred again at the downstream edge but with a higher frequency and shorter burst period (typically 0.025 s). The

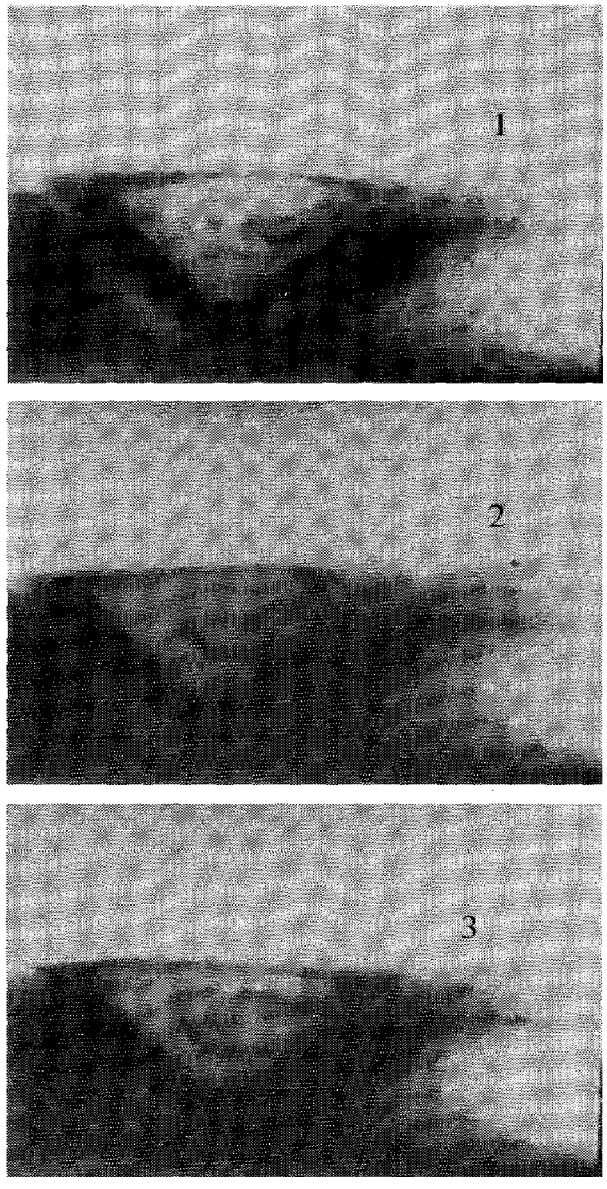

FIG. 8. Photographs showing the sequential changes in the flow pattern within the larger groove at $Re = 10\,800$ during fluid entrainment process and at the start of the ejection phase.

nature of the intermediate stages also changed from cycle to cycle, with the inflow phase occurring predominantly in a very smooth manner in contrast to the outflow phase that occurred quite abruptly. In general, a small vortex was seen to develop within the downstream half of the groove, and this eventually led to the orderly ejection phase as shown in Fig. 8. As the fluid became entrained along the downstream slope, it circulated in the clockwise direction. This process continued until just prior to the burst or ejection when, as the high speed fluid was being swept down the slope, it appeared to impact upon the slower moving fluid at the bottom of the groove (Fig. 8) and was deflected in such a manner that a kink in the trace was produced. A counterclockwise motion was then superimposed on the clockwise circulation and fluid ejection ensued.

Figure 9a shows the pattern during a quiescent period when there was no fluid exchange. It is possible for the smooth inflow of fluid to be associated simultaneously with a smooth outflow in the same plane of view or with ejection at a different spanwise location. However, during the strong ejection phase just described (Fig. 9b), the flow in the plane of view was mainly outflow. Thus, during the burst period, the inflow and outflow phases occurred at least at two different spanwise locations. At higher Reynolds numbers of 20 500 or 22 500 and with either groove, the exchange process was similar to that at $Re =$ 10 800, except that the burst frequency was higher and the duration of the various stages was shorter.

In order to obtain further insight on the dynamics of the fluid exchange processes, we examined the motion of the interface that apparently separated the fluid within the groove from that of the bulk flow. This was achieved by placing the dye trace within the groove itself and observing its motion over longer periods than those used in the calculation of the vel-

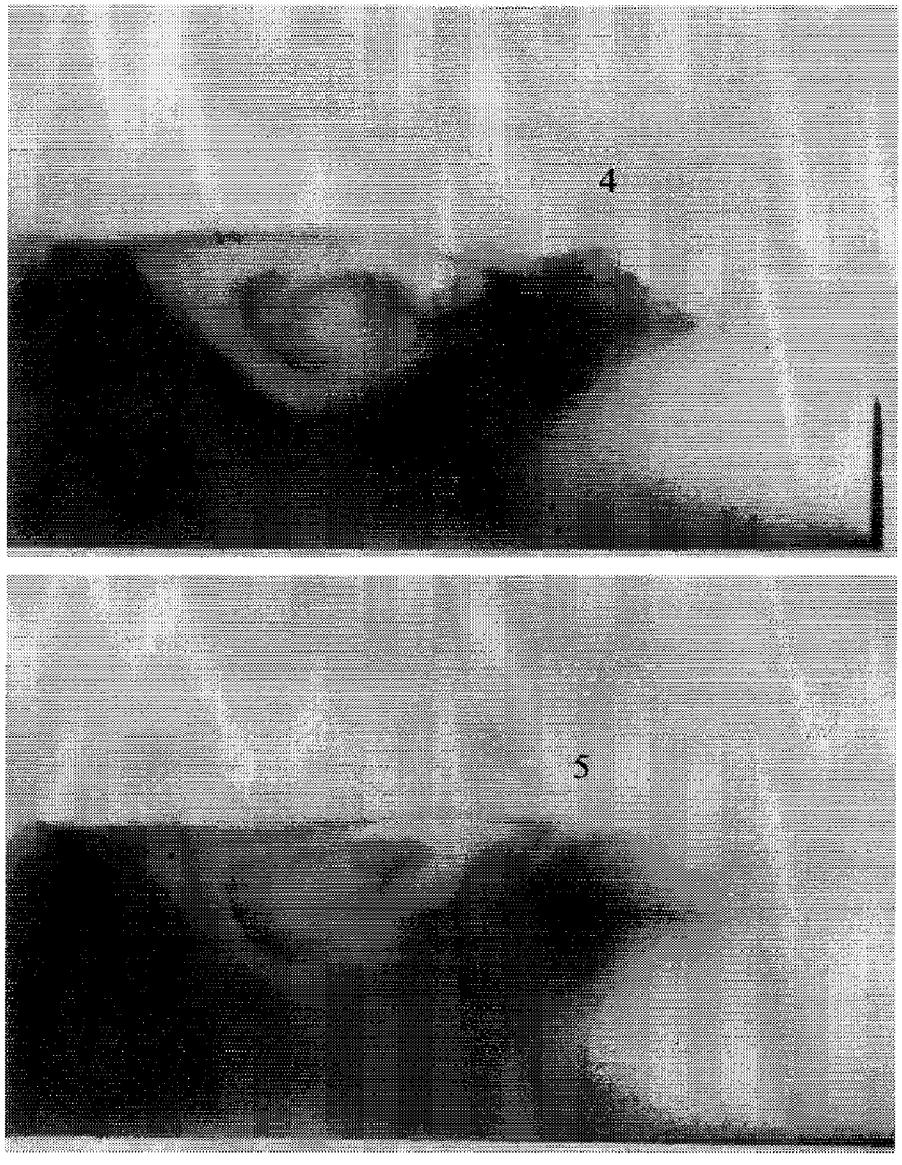

FIG. 8—*continued.*

ocities. Examples of the position of the interface were shown earlier in Figs. 8 and 9. During the quiescent period, as displayed in Fig. 9a, the interface oscillated with a relatively low frequency and amplitude. The downstream end displayed a pattern similar to that of a "wagging fish tail". Additional information on the interface motion was obtained by determining its height with respect to the line joining the two edges. A three-dimensional representation of the results is shown in Fig. 10: time-dependence of the shape of the interface profile. This dynamic pattern of the interface was obtained by digitizing 480 sequential frames recorded at a rate of 1000 frames s^{-1}.

Again, the strong asymmetry in the flow field within the groove is quite evident with most of the activity occurring in the downstream section. The valleys and hills signify inflow and outflow, respectively. In general, the exchange process was quite periodic. The wave-like motion was usually initiated at the upstream edge and the time taken for this motion to reach the downstream edge was time-dependent. For example, around frame numbers 40 and 250, the time intervals were 5 and 10 ms, respectively. Quite vigorous multiple ejections were occasionally observed as shown in frames 35–60.

During the ejection phase of the bursting process, fluid from within the groove with very low velocities in the axial direction would be pushed outwards, thereby causing a reduction in the magnitude of the axial velocity over the groove. Since the ejection phase was much shorter than the interval between successive ejections, the time-averaged axial velocities would be higher than the instantaneous axial velocities during the ejection phase. Figure 10b shows a comparison of the instantaneous axial profiles with the mean profile for the three different instants indicated in Fig. 10a. For each occasion, three successive instantaneous axial profiles are compared with the mean profile. The first sequence (A) was chosen when the ejection of fluid was not apparent; consequently, the instantaneous velocities were larger than the mean value. However, with fluid ejection, as occurred during the second and third sequences (B and C), the instantaneous values were smaller than the mean. The velocity fluctuations were often 25–50% of the mean value, which is typical of those seen in the near-wall region for smooth surfaces. This resulted in the high levels of turbulence intensities over the groove as discussed earlier for Fig. 7b.

A Fourier analysis was performed on the interface data (position vs time) to determine the periodic nature of the fluid exchange process. One upstream and five downstream locations were chosen: $X = 0.14$, 0.65, 0.68, 0.72, 0.76 and 0.79, where X is the distance from the upstream edge of the groove normalized with respect to the width (axial dimension) of the groove. The downstream region of the interface was emphasized since it corresponded to the region where most of the exchange occurred. The results for $X = 0.79$ are displayed in Fig. 11; the pattern seen with the other

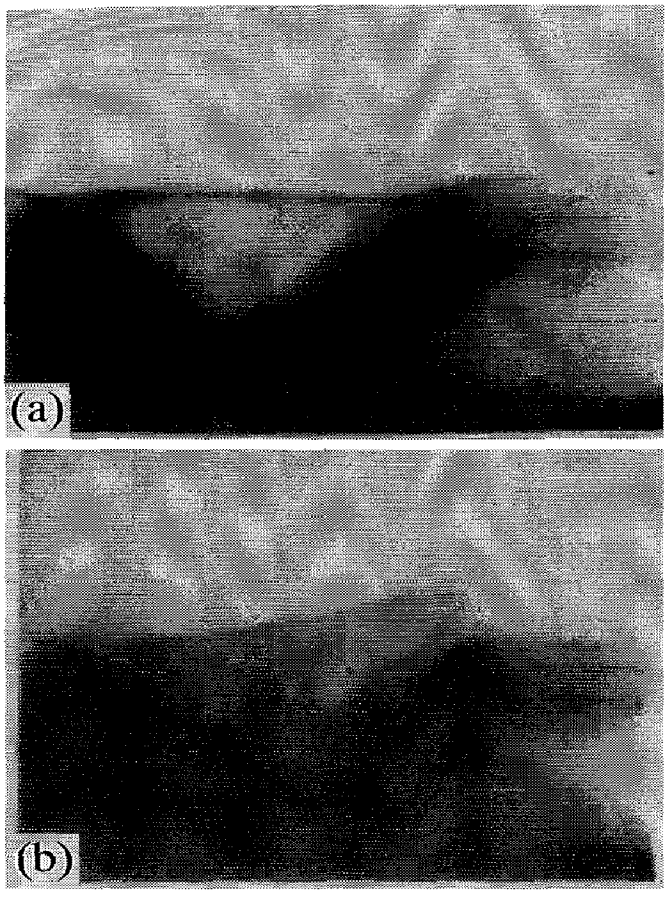

FIG. 9. Photographs of the flow pattern during: (a) a quiescent period; and (b) an abrupt ejection.

downstream locations was similar. Each periodogram showed two distinct peaks at 0.026 and 0.17 s, except for the upstream location which showed one peak at 0.026 s, again signifying that the exchange was confined mainly to the downstream section of the groove. The larger period was due to the gentle oscillation of the interface and the smaller one corresponded to the interval between successive bursts.

Figure 12 shows the relationship between burst period (interval between two successive bursts) and friction velocity for smooth surfaces as predicted by the empirical equation of Heidrick *et al.* [27]. The burst period for the V-shaped groove is also plotted and a nearly twofold increase in the burst frequency is seen compared to the smooth surface results. The smooth surface value for the friction velocity was used here; an allowance for the effect of the groove as a roughness element that increases pressure losses would increase the u^* value, thereby shifting the point towards the general trend.

DISCUSSION

Drag reduction by longitudinal grooves appears to be due to premature bursts that occur at higher frequencies than those observed with smooth surfaces at equivalent Reynolds numbers [10]. Consequently,

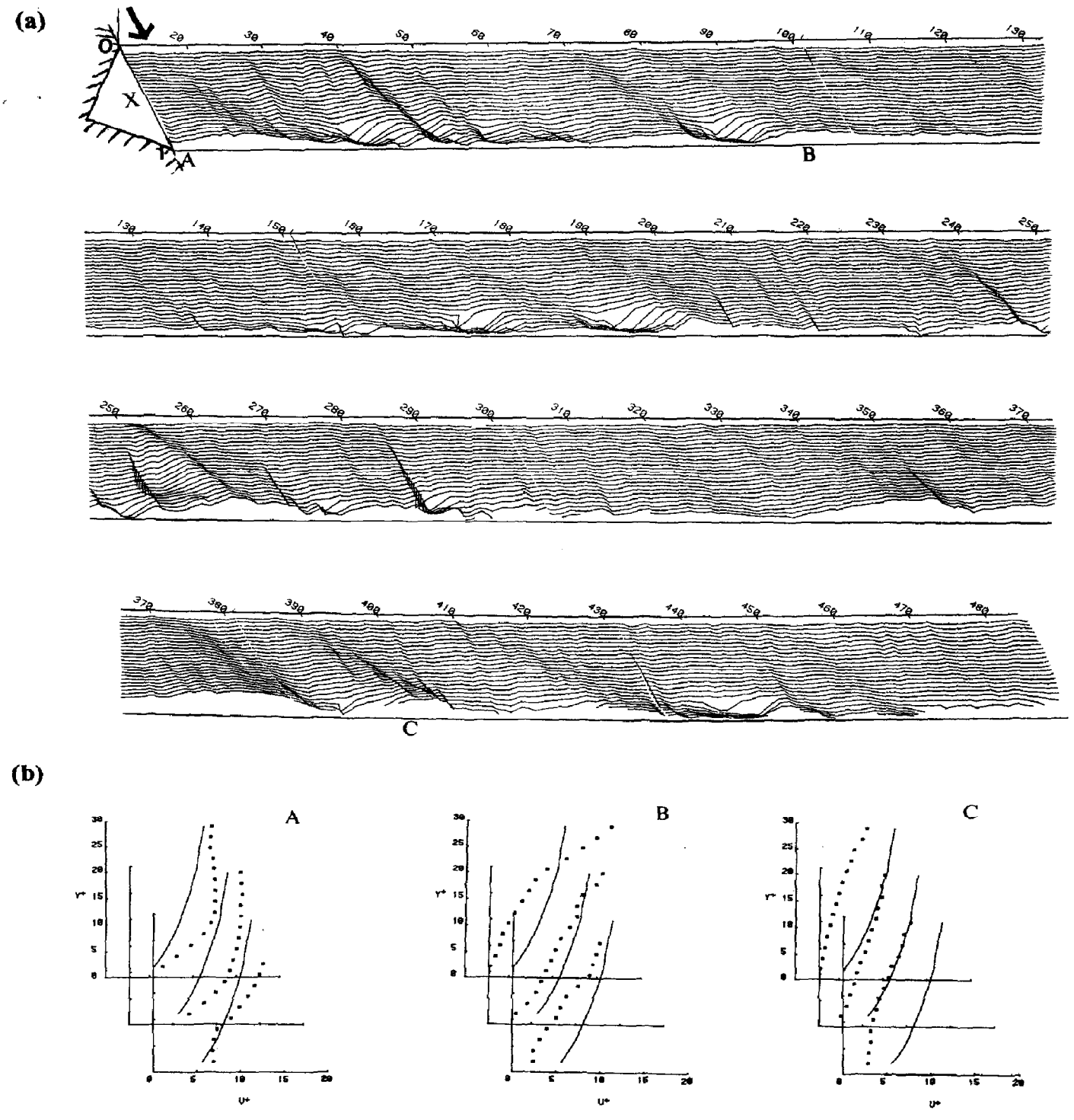

FIG. 10. (a) Dynamic behavior of the interface over the larger groove for $Re = 10\,800$. The height of the interface above the smooth surface is plotted as a function of axial distance from the upstream edge and frame number (with the interval between successive frames being 1 ms). The axial distance X is normalized with respect to the groove width. (b) Three sequences of instantaneous trace displacement profiles vs the mean profile (solid line) taken at times indicated in (a).

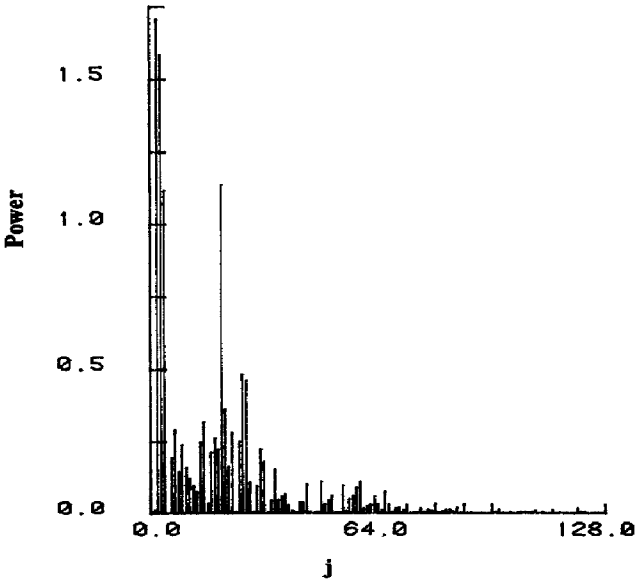

FIG. 11. Periodogram showing the relative strength of the various harmonics associated with the interface movements at $X = 0.79$ for the large groove at $Re = 10\,800$. Frequency (radians s^{-1}) $= 2\pi j/512$ for the jth harmonic.

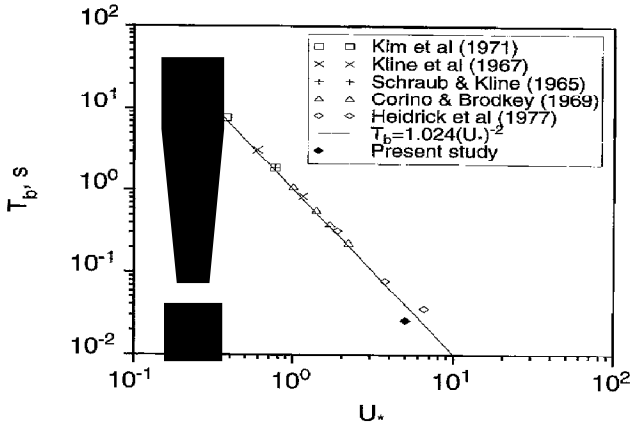

Fig. 12. Functional dependence of burst period (interval between consecutive bursts) on friction velocity as reported by Heidrick *et al.* [27]. The result from the present study is also shown.

with such grooves, the mean velocity profile is shifted upwards and the turbulence intensity profile is shifted downwards with respect to the profiles seen with smooth surfaces. In the present study, single V-shaped grooves oriented transversely resulted in the mean velocity profile being parallel to the outer region profile seen with smooth surfaces. That is, the near-wall velocities were higher, and, further out, the velocities were lower. Also, higher turbulence intensities were seen in the near-wall region and with the larger groove at $Re = 10\,800$, the burst frequency appeared to be higher than that for a smooth surface. It is therefore possible that the enhancement in mass transfer by transverse grooves is due to the increased intensity of the individual bursts and to an increased burst frequency. While both will lead to higher frictional losses, the mass transfer enhancement at high Schmidt numbers is much greater, as demonstrated by Dawson and Trass [15].

The liquid exchange process was found to be basically periodic, and, for $Re = 10\,800$, the ejection phase was triggered by the formation of a counter-rotating vortex superimposed on the main rotation within the groove. For smooth surfaces, the mean burst period is proportional to $(u^*)^{-2}$ [27]. Recently, Bandyopadhyay [28] and Klebanoff *et al.* [29] reported a similar functional dependency of the mean burst period with the friction velocity using two- and three-dimensional surfaces and with the roughness pattern being either regular or random. As noted earlier, the mean burst period was determined only at $Re = 10\,800$ for the large groove in the present study, and it was found to be slightly smaller than that for smooth surfaces.

This study focused on a single groove embedded in a smooth surface. With multiple grooves, the exchange process will no doubt be different since the downstream grooves will be subjected to different inlet velocity fields and also because of the likely interactions between adjacent grooves. The results from the present study may be useful in assessing the extent of such interactions.

Acknowledgements—Financial support from the Natural Sciences and Engineering Research Council of Canada is appreciated. Sunil Tantirige was a recipient of a University of Toronto Open Fellowship.

REFERENCES

1. L. C. Thomas, A turbulent burst model of wall turbulence for two-dimensional turbulent boundary layer flow, *Int. J. Heat Mass Transfer* **25,** 1127–1136 (1982).
2. S. J. Kline, W. C. Reynolds, F. A. Schraub and P. W. Runstadler, The structure of turbulent boundary layers, *J. Fluid Mech.* **30,** 741–773 (1967).
3. A. E. Corino and R. S. Brodkey, A visual investigation of the wall region in turbulent flow, *J. Fluid Mech.* **37,** 1–30 (1969).
4. H. T. Kim, S. J. Kline and W. C. Reynolds, The production of turbulence near a smooth wall in a turbulent boundary layer, *J. Fluid Mech.* **50,** 133–160 (1971).
5. A. J. Grass, Structural features of turbulent boundary layer flow over smooth and rough surfaces, *J. Fluid Mech.* **50,** 231–250 (1971).
6. T. S. Lutchik and W. G. Tiederman, Time-scale and structure of ejections and bursts in turbulent channel flows, *J. Fluid Mech.* **174,** 529–552 (1987).
7. M. S. Acalar and C. R. Smith, A study of hairpin vortices in a laminar boundary layer. Part 2. Hairpin vortices generated by fluid injection. *J. Fluid Mech.* **175,** 43–83 (1987).
8. J. O. Hinze, *Turbulence*, 2nd Edn. McGraw-Hill, New York (1975).
9. M. J. Walsh, Drag characteristics of V-groove and transverse curvature riblets. In *Viscous Drag Reduction* (Edited by G. R. Hough). American Institute of Aeronautics and Astronautics (1980).
10. K.-S. Choi, Near wall structure of a turbulent boundary layer with riblets, *J. Fluid Mech.* **208,** 417–458 (1989).
11. E. F. Matthys, Some recent developments in convective heat transfer to drag reducing fluids. In *Drag Reduction in Fluid Flows: Techniques for Friction Control* (Edited

by R. H. J. Sellin and R. T. Moses), pp. 129–139. Ellis Horwood, West Sussex (1989).
12. J. C. Han, S. Ou, J. S. Park, and C. K. Lei, Augmented heat transfer in rectangular channels of narrow aspect ratios with rib turbulators, *Int. J. Heat Mass Transfer* **32,** 1619–1630 (1989).
13. M. Molki and A. R. Mostoufizadeh, Turbulent heat transfer in rectangular ducts with repeated-baffle blockages, *Int. J. Heat Mass Transfer* **32,** 1491–1499 (1989).
14. I. S. Kang and H. N. Chang, The effect of turbulence promoters on mass transfer—numerical analysis and flow visualization, *Int. J. Heat Mass Transfer* **25,** 1167–1181 (1982).
15. D. A. Dawson and O. Trass, Mass transfer at rough surfaces, *Int. J. Heat Mass Transfer* **15,** 1317–1336 (1972).
16. A. T. Popovich and R. L. Hummel, Experimental study of the viscous sublayer in turbulent pipe flow, *A.I.Ch.E. Jl* **13,** 854–860 (1967).
17. A. Iribarne, F. Frantisak, R. L. Hummel and J. W. Smith, An experimental study of instabilities and other flow properties of a laminar pipe jet, *A.I.Ch.E. Jl* **18,** 689–698 (1972).
18. L. E. Seeley, J. W. Smith and R. L. Hummel, Experimental velocity profiles in laminar flow around a sphere at intermediate Reynolds numbers, *J. Fluid Mech.* **68,** 591–608 (1975).
19. S. Dunn and J. W. Smith, Some statistical properties of turbulent momentum transfer in rough pipes, *Can. J. Chem. Eng.* **50,** 561–568 (1972).
20. M. Ojha, R. L. Hummel, R. S. C. Cobbold and K. W. Johnston, Development and evaluation of a high resolution photochromic dye method for pulsatile flow studies. *J. Physics: E. Scientific Instruments* **21,** 998–1004 (1988).
21. M. Ojha, R. S. C. Cobbold, K. W. Johnston and R. L. Hummel, Pulsatile flow through constricted tubes: an experimental investigation using photochromic tracer methods, *J. Fluid Mech.* **203,** 173–197 (1989).
22. H. Schlichting, *Boundary Layer Theory*, 7th Edn. McGraw-Hill, New York (1979).
23. S. C. Tantirige, A flow visualization investigation of the turbulent boundary layer over regularly rough surfaces, Ph.D. Thesis, University of Toronto (1989).
24. T. von Karman, The analogy between fluid friction and heat transfer. *Trans ASME* **61,** 705–710 (1939).
25. W. R. B. Morrison and R. E. Kronauer, Structural similarity for fully developed turbulence in smooth tubes, *J. Fluid Mech.* **39,** 117–141 (1969).
26. H. Ueda and J. O. Hinze, Fine structure turbulence in the wall region of a turbulent boundary layer. Part 1, *J. Fluid Mech.* **67,** 125–143 (1975).
27. T. R. Heidrick, S. Banerjee and R. S. Azad, Experiments on the structure of turbulence in fully developed pipe flow. Part 2: A statistical procedure for identifying the bursts in the wall layers and some characteristics of flow during the bursting periods, *J. Fluid Mech.* **82,** 705–723 (1977).
28. D. R. Bandyopadhyay, Rough wall turbulent boundary layers in the transition regime, *J. Fluid Mech.* **180,** 231–266 (1987).
29. P. S. Klebanoff, W. G. Cleveland and K. D. Tindstrom, On the three-dimensional roughness and evolution of a turbulent boundary layer, AEDC TR-87-7 (1987).